AIAA 82-4242

# Transonic Flutter and Response Analyses of Two 3-Degree-of-Freedom Airfoils

T.Y. Yang* and C.H. Chen†
*Purdue University, West Lafayette, Indiana*

**Flutter and time-response analyses are performed for a NACA 64A006 conventional and a MBB A-3 supercritical airfoil, both oscillating with plunge, pitch, and aileron pitch degrees-of-freedom (DOF's) in small-disturbance transonic flow. The aerodynamic coefficients are calculated using the transonic code LTRAN2-NLR. The effects of various kinds of aeroelastic parameters on flutter speeds for the bending-torsion, bending-aileron, and torsion-aileron branches are studied. The flutter speeds associated with the bending-torsion branch are plotted against Mach number for different parameter values and the transonic dip phenomenon is demonstrated. To study the flutter modes, the flutter speed, amplitude ratio, and phase difference at different Mach numbers are plotted against the mass ratio for both a 2DOF and a 3DOF case. Time-response results are obtained for the NACA 64A006 and the MBB A-3 airfoils at $M=0.85$ and 0.765, respectively. Based on the same sets of parameter values, the flight speeds used to obtain all the neutrally stable responses are very close to the flutter speeds obtained in the flutter analysis. The principle of linear superposition of airloads is used in the flutter analysis, but not in the response analysis.**

## Introduction

THE numerical methods and computer codes for transonic unsteady aerodynamics have been developed significantly in recent years. A state-of-the-art review of the numerical methods was given by Ballhaus and Bridgeman.[1] Aeroelastic applications of these developments were performed and reviewed by authors such as Ashley,[2] and Yang, Guruswamy, and Striz.[3] Extensive reviews and physical interpretations of the transonic flutter problems of wings were given by Mykytow[4] and Zwaan.[5]

Farmer and Hanson[6] performed flutter model tests and analyses of two dynamically similar wings, one with supercritical sections and the other with conventional sections. It was found that the experimental results agreed with those calculated from the subsonic lifting surface theory up to the Mach number of 0.85. Beyond that Mach number, the experimental curves for dynamic pressure showed a transonic dip phenomenon and the supercritical wing experienced a much more pronounced transonic dip than the conventional wing.

Flutter analyses of airfoils oscillating with only two DOF's (plunge and pitch) were carried out extensively. Rizzetta[7] used STRANS2 and UTRANS2[8] to analyze a NACA 64A010 airfoil. Yang, Striz, Guruswamy, and Olsen used STRANS2, UTRANS2, and LTRAN2[9] to analyze a NACA 64A006 airfoil.[10] Yang, Guruswamy, and Striz later used both codes to analyze a MBB A-3,[11] and a NACA 64A010[3] airfoil. They also used LTRAN2 to analyze a CAST 7 airfoil and used STRANS2 and UTRANS2 to analyze a TF-8A wing section.[3] Owing to the low-frequency approximation used in LTRAN2 and the convergence difficulty encountered in using UTRANS2, the reduced frequencies in full chord were restricted to within approximately 0.2 or 0.3, thus limiting the ranges of aerodynamic and aeroelastic parameters chosen.

Reviews of flutter examples of a straight, a swept, and a delta cantilevered wing in Refs. 4 and 5 suggested that the transonic flutter characteristics of the swept wing emerge as most critical. The first bending and first torsion natural vibration modes and the nodal lines for a swept-back wing are plotted in common literature (see, for example, Fig. 7 of Ref. 5). For a typical swept-back wing section vibrating in the first bending mode, the pivot point is ahead of the leading edge.[5,12,13] In the analysis of such a section, Isogai[12] suggested that the mechanism of the single DOF (first natural mode) flutter dominates the flutter of the system studied at the bottom of the transonic dip. The large time lag between the aerodynamic pressure and the airfoil motion in the transonic region, which is caused by the compressibility effect, is the main cause of the transonic dip phenomenon. Isogai[13] also developed a transonic small-perturbation code which can be used for the reduced frequency $k_c$ with values up to 1.0 and the entire transonic Mach number range. He used the code to study the NACA 64A010 airfoil for two cases, simulating characteristics of a streamwise section of a swept-back and an unswept wing. It was suggested from the examination of the unsteady load distributions that the large negative damping produced by the phase lag of the shock wave motion is the cause of the occurrence of the single DOF (first natural mode) flutter and hence the cause of the transonic dip phenomenon.

McGrew et al.[14] carried out flutter analysis of a TF-8A flutter model and the YC-15II prototype aircraft. It was demonstrated that supercritical wings exhibited significantly lower flutter speeds than a conventional wing of equal size and rigidity.

Eastep and Olson[15] reported the flutter analysis of a rectangular wing by using the three-dimensional unsteady transonic codes TDSTRN and TDUTRN.[8]

In addition to the flutter analysis, aeroelastic time-response analysis has also become a topic of recent interest. Ballhaus and Goorjian[16] first performed a time-response analysis of a NACA 64A006 airfoil oscillating with a pitch DOF at $M=0.88$. The time-response analysis was computed by using their program LTRAN2 for unsteady flow coupled with an integration procedure for the structural equation of motion.

Rizzetta[17] performed a time-response analysis of a NACA 64A010 airfoil with a single pitch DOF and three DOF's—pitch, plunge, and aileron pitch. The LTRAN2 code was used. It was pointed out in Ref. 17 that no attempt was made to obtain the neutrally stable response curves corresponding to the flutter condition for the 3DOF system.

Guruswamy and Yang[18] performed a time-response analysis of a flat plate (at $M=0.7$) and a NACA 64A006 airfoil (at $M=0.85$) oscillating with plunge and pitch DOF's. Again, LTRAN2 was used. Parameters that resulted in the

Received June 19, 1981; revision received Nov. 30, 1981. Copyright © American Institute of Aeronautics and Astronautics, Inc., 1981. All rights reserved.

*Professor and Head, School of Aeronautics and Astronautics. Associate Fellow AIAA.

†Graduate Student, School of Aeronautics and Astronautics.

neutrally stable response agreed with those equivalent to the flutter conditions found in a separate flutter analysis. The principle of linear superposition of airloads was used in the flutter analysis but not in the response analysis.

Recently, several modifications have been incorporated into LTRAN2. Houwink and van der Vooren[19] improved the LTRAN2 code by developing its NLR (National Aerospace Laboratory of the Netherlands) version. High-frequency terms were added to the boundary conditions and the pressure computations. Rizzetta and Chin[20] and Rizzetta and Yoshihara[21] included the $\phi_{tt}$ term in the small-disturbance equation. There is no longer the assumption of low reduced frequency. Viscous effects were incorporated in the code by using a viscous ramp method.[21]

Goorjian[22] gave a preliminary study to remove the small-disturbance and low-frequency restrictions by considering the full potential equation. Borland, Rizzetta, and Yoshihara[23] developed a transonic code LTRAN3 which can solve the three-dimensional low-frequency, unsteady transonic equation by the time-integration method.

Among these new developments, the LTRAN2-NLR appears to be an attractive code for aeroelastic applications. In the computation of the unsteady aerodynamic coefficients, the LTRAN2-NLR can be applied to a considerably extended range of reduced frequency as compared to LTRAN2 and UTRANS2. With this new capability, the flutter analysis and the time-response predictions for the 3DOF (plunge, pitch, and aileron pitch) systems become more feasible. More realistic and broader ranges of parameter values can be considered.

In this study, LTRAN2-NLR is used to analyze a NACA 64A006 conventional and a MBB A-3 supercritical airfoil fitted with trailing-edge ailerons of 25% of the chords. Three DOF's are considered. Flutter analysis is first performed and the effects of various parameters are studied. Transonic dip phenomenon is observed and discussed. The neutrally stable time-response predictions are then obtained with their flight speeds correlated to the flutter speeds found in the flutter analysis. The effect of the mass ratio on the flutter modes (amplitude ratios and phase differences) for various Mach numbers is studied.

## Flutter Equation and Solution Procedure

The parameters and sign conventions for the airfoil with pitch, plunge, and aileron pitch DOF's are defined in Fig. 1. The system is similar to that discussed in Sec. 6.10 of Ref. 24.

Based on the derivations given in Ref. 24 the flutter equation can be written in the form

$$\left[\frac{1}{4}\mu k_c^2[M]-\frac{1}{\pi}[A]\right]\begin{Bmatrix}\xi\\ \alpha\\ \beta\end{Bmatrix}=\lambda[K]\begin{Bmatrix}\xi\\ \alpha\\ \beta\end{Bmatrix} \tag{1}$$

where $\mu=m/\pi\rho b^2$ is the mass ratio; $k_c=\omega c/U$ is the reduced frequency; $\xi=h/b$ is the nondimensional plunge displacement; the three matrices are defined as

$$[M]=\begin{bmatrix}1 & x_\alpha & x_\beta\\ x_\alpha & r_\alpha^2 & (c_\beta-a_h)x_\beta+r_\beta^2\\ x_\beta & (c_\beta-a_h)x_\beta+r_\beta^2 & r_\beta^2\end{bmatrix}$$

$$[A]=\begin{bmatrix}\tfrac{1}{2}c_{l\delta} & c_{l\alpha} & c_{l\beta}\\ -c_{m\delta} & -2c_{m\alpha} & -2c_{m\beta}\\ -c_{n\delta} & -2c_{n\alpha} & -2c_{n\beta}\end{bmatrix} \tag{2a}$$

$$[K]=\begin{bmatrix}(\omega_h/\omega_r)^2 & 0 & 0\\ 0 & r_\alpha^2(\omega_\alpha/\omega_r)^2 & 0\\ 0 & 0 & r_\beta^2(\omega_\beta/\omega_r)^2\end{bmatrix} \tag{2b}$$

(2c)

where $r_\alpha=(I_\alpha/mb^2)^{1/2}$ and $r_\beta=(I_\beta/mb^2)^{1/2}$ are the radii of gyration of the airfoil and aileron about the elastic axis and the aileron hinge axis, respectively; matrix $[A]$ contains the nine aerodynamic coefficients associated with the three respective DOF's; $\omega_h=(K_h/m)^{1/2}$, $\omega_\alpha=(K_\alpha/I_\alpha)^{1/2}$, $\omega_\beta=(K_\beta/I_\beta)^{1/2}$ are the three uncoupled natural frequencies; and $\omega_r=\omega_\alpha$ is the reference frequency.

The eigenvalue $\lambda$ is a complex number defined as

$$\lambda=\mu(1+ig)\omega_r^2b^2/U^2 \tag{3}$$

where $g$ is the so-called structural damping coefficient. The flutter solution is obtained when $g$ is found to be zero.[24] The flutter speed is nondimensionalized as $U^*=U/b\omega_\alpha=(\omega_r/\omega_\alpha)\sqrt{\mu/\lambda}$.

In the present flutter analysis, the principle of linear superposition of airloads was assumed valid in deriving the flutter equation.

Justification of this principle was studied experimentally by Davis and Malcolm[25] for a NACA 64A010 airfoil oscillating with plunge and pitch DOF's. In the conclusion, they stated that the principles of superposition and linearity were shown to be valid for supercritical attached flow. In a time-response analysis of a NACA 64A006 airfoil oscillating with plunge and pitch DOF's, Guruswamy and Yang[18] showed in a specific example that the parameter values associated with the flutter speed at the bottom of a transonic dip can indeed be used to obtain the neutrally stable response. The principle of superposition was used in the flutter analysis but not in the response analysis.

As an attempt to validate this principle in its application to flutter analysis of 3DOF case, neutrally stable response results are obtained for three specific examples where alternative flutter solutions are found in the separate flutter analyses.

In the flutter analysis, the elastic axis does not always coincide with the pitching axis for which the aerodynamic data are obtained. The equations for transforming the aerodynamic coefficients for a pitching axis 0′ (see Fig. 1) to those for another pitching axis (elastic axis) 0 are in the following form[8]:

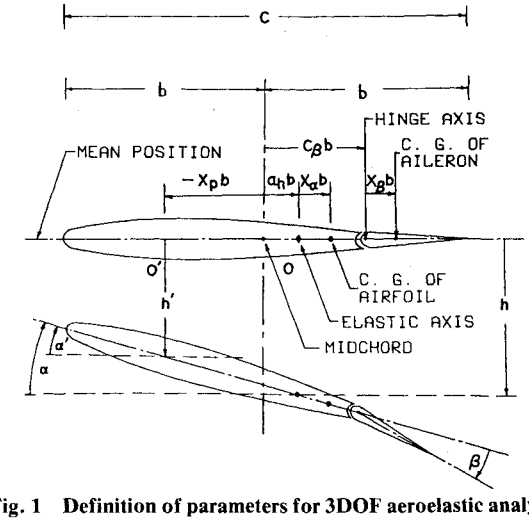


**Fig. 1 Definition of parameters for 3DOF aeroelastic analysis.**

$$c_{l\delta}=c_{l\delta}' \quad c_{l\alpha}=c_{l\alpha}'-sc_{l\delta}' \quad c_{l\beta}=c_{l\beta}'$$

$$c_{n\delta}=c_{n\delta}' \quad c_{n\alpha}=c_{n\alpha}'-sc_{n\delta}' \quad c_{n\beta}=c_{n\beta}'$$

$$c_{m\delta}=c_{m\delta}'+sc_{l\delta}' \quad c_{m\alpha}=c_{m\alpha}'+s(c_{l\alpha}'-c_{m\delta}')-s^2c_{l\delta}'$$

$$c_{m\beta}=c_{m\beta}'+sc_{l\beta}' \tag{4}$$

where $s=(a_h-x_p)/2$.

## Equations of Motion and Response Analysis Procedure

The time-response analysis is based on the following equations of motion:

$$[M]\begin{Bmatrix}\xi''\\ \alpha''\\ \beta''\end{Bmatrix}+\left(\frac{2\omega_r}{U^*k_c\omega_\alpha}\right)^2[K]\begin{Bmatrix}\xi\\ \alpha\\ \beta\end{Bmatrix}$$

$$=\left(\frac{4}{\pi\mu k_c^2}\right)\begin{Bmatrix}-c_l\\ 2c_m\\ 2c_n\end{Bmatrix} \tag{5}$$

where the prime indicates derivative with respect to non-dimensional time $\bar{t}(=\omega t)$.

Equation (5) can be written in a simplified symbolic form as

$$[M]\{q''\}+[N]\{q\}=\{p\} \tag{6}$$

where $\{q\}$ is the vector for the three DOF's; $[N]=(2\omega_r/U^*k_c\omega_\alpha)^2[K]$; and $\{p\}$ is the vector of aerodynamic forces. This equation can be solved by a step-by-step time-integration finite-difference approach.

Assuming a linear variation of acceleration, the velocities and displacements after a small time step $\Delta t$ can be expressed as

$$\{q'\}_t=\{q'\}_{t-\Delta t}+(\Delta t/2)\{q''\}_{t-\Delta t}+(\Delta t/2)\{q''\}_t$$

$$\{q\}_t=\{q\}_{t-\Delta t}+\Delta t\{q'\}_{t-\Delta t}+(\Delta t^2/3)\{q''\}_{t-\Delta t}$$

$$+(\Delta t^2/6)\{q''\}_t \tag{7}$$

Substituting Eqs. (7) into Eq. (6) yields

$$\{q''\}_t=[F]\left[\{p\}_{t-\Delta t}-[N]\{r\}\right] \tag{8}$$

where

$$[F]=\left[[M]+(\Delta t^2/6)[N]\right]^{-1} \tag{9a}$$

$$\{r\}=\{q\}_{t-\Delta t}+\Delta t\{q'\}_{t-\Delta t}+(\Delta t^2/3)\{q''\}_{t-\Delta t} \tag{9b}$$

This direct integration method for structural response analysis is well known.[26] The vector for aerodynamic forces is obtained using LTRAN2-NLR code.

In each time step, $\{q''\}$ at the time $t$ are first obtained from the known values of $\{q\}$, $\{q'\}$, $\{q''\}$, and $\{p\}$ at $t-\Delta t$ from Eq. (8). The vectors $\{q'\}$ and $\{q\}$ at the time $t$ are then obtained from Eqs. (7). Based on the known values of $\{q\}$ and $\{q'\}$, the aerodynamic force vector $\{p\}$ at the time $t$ can be obtained using LTRAN2-NLR code. A detailed description of the time-response analysis procedure is given in Ref. 18.

In order to obtain the neutrally stable responses for flutter condition earlier, the aerodynamic equation alone may be integrated in time for several cycles in response to the forced motion. The displacement vector of the airfoil is specified according to the amplitude ratios and the phase angles of the flutter mode of the 3DOF system. After the aerodynamic responses become periodic, the system is set free, the simultaneous integration procedure begins, and the airfoil and the aerodynamic forces drive each other.

## Results of Aerodynamic Computations

A NACA 64A006 conventional and a MBB A-3 supercritical airfoil were studied. Both configurations were among those proposed by AGARD for aeroelastic applications of transonic unsteady aerodynamics. The airfoil coordinates used were taken from Ref. 27. Both the steady and unsteady aerodynamic coefficients were computed by using LTRAN2-NLR code.[19]

In view of the strong dependence of unsteady loads on the steady aerodynamics in the transonic range, the first step is to assure that the pressure distribution and magnitude for the steady case, including shock location and strength are correct. The next step is then incorporation of the effects of frequency on magnitude and phase angle of the shock motions and of overall aerodynamic forces.

Figure 2 shows the steady pressure distributions for the NACA 64A006 airfoil with zero angle of attack for $M=0.7$, 0.8, 0.85, 0.875. The experimental results obtained by Tijdeman[28] at $M=0.85$ were also plotted. At $M=0.85$, a weak shock wave is present. The present results agree well with those by Tijdeman except in the neighborhood of 30~40% of the chord. At $M=0.875$, a strong shock wave is formed.

The design conditions for the MBB A-3 airfoil are: $M=0.765$; $c_l=0.58$; $\alpha=1.3$ deg. In an attempt to match the design lift coefficient of 0.58, the angles of attack were chosen as 1.2, 1.2, 0.86, and 0.6 deg for Mach numbers 0.7, 0.74, 0.765, and 0.78, respectively. The steady pressure distributions for the four cases were plotted in Fig. 3. The experimental results of Bucciantini, Oggiano, and Onorato[29] obtained in the A.R.A. Bedford Wind Tunnel for $M=0.765$, $c_l=0.519$, and $\alpha=1.5$ deg were also plotted. For $M=0.765$, a relatively weak shock wave occurs in the neighborhood of 55~60% of the chord. The results agree well with the experimental data except in the neighborhood of 40~60% of the chord. The present angle of attack is, however, smaller than that used in Ref. 29. For $M=0.78$, the shock wave becomes stronger and shifts aft.

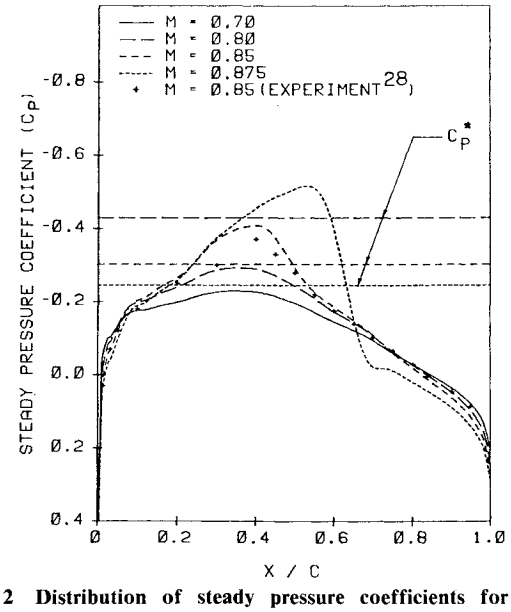


**Fig. 2 Distribution of steady pressure coefficients for NACA 64A006 airfoil.**

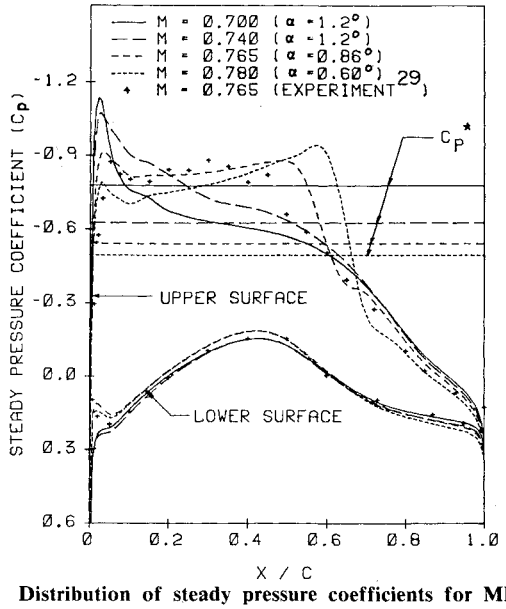


**Fig. 3 Distribution of steady pressure coefficients for MBB A-3 airfoil with $c_l \simeq 0.58$.**

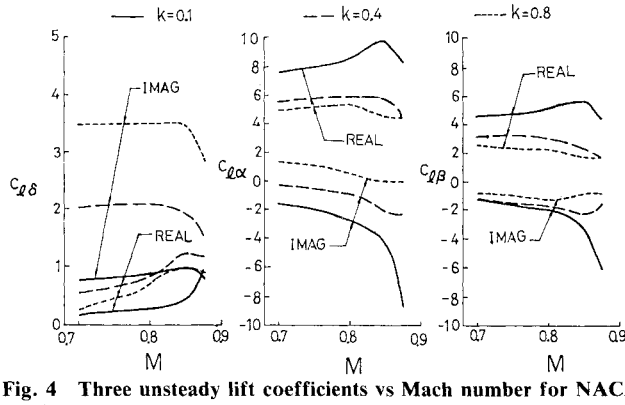


**Fig. 4 Three unsteady lift coefficients vs Mach number for NACA 64A006 airfoil at three reduced frequencies.**

In the unsteady aerodynamic calculations, 60 time steps were used for each half-cycle. The amplitudes chosen were 0.02 chord and 0.1 deg for the plunge and pitch DOF's, respectively. The nine aerodynamic coefficients $c_{l\delta}$, $c_{l\alpha}$, $c_{l\beta}$, $c_{m\delta}$, $c_{m\alpha}$, $c_{m\beta}$, $c_{n\delta}$, $c_{n\alpha}$, and $c_{n\beta}$, were computed by using a $79 \times 99$ grid. Both airfoils fitted with trailing-edge ailerons of 25% of the chords were assumed to pitch about the quarter chord. The results were tabulated in Ref. 30 with reduced frequency $k_c$ equal to 0.1, 0.2, 0.3, 0.4, 0.6, 0.8, 1.2, and 1.6 for each Mach number considered. Figures 4-6 show the trends for the nine aerodynamic coefficients (both real and imaginary) vs Mach number for NACA 64A006 airfoil at three different values of reduced frequency.

## Results of Flutter Analysis

Unless otherwise specified, the present flutter analysis was based on the following set of common parameters: $a_h = -0.2$; $x_\alpha = 0.2$; $r_\alpha = 0.5$; $x_\beta = 0.008$; $r_\beta = 0.06$; $\omega_h/\omega_\alpha = 0.3$; and $\mu = 50$. The Mach numbers considered were 0.7, 0.8, 0.85, and 0.875 for the NACA 64A006 airfoil and 0.7, 0.74, 0.765, and 0.78 for the MBB A-3 airfoil. A flutter analysis of a flat plate with a trailing-edge aileron at $M = 0.7$ was first performed using the aerodynamic data obtained from the kernel function method and LTRAN2-NLR code. The two sets of curves obtained for $U^*$ vs $\omega_\beta/\omega_\alpha$ by the two methods agreed well with each other.[30]

### Effect of Frequency Ratios $\omega_\beta/\omega_\alpha$ and $\omega_h/\omega_\alpha$

The curves for the flutter speed vs $\omega_\beta/\omega_\alpha$ ranging from 0 to 2 for three $\omega_h/\omega_\alpha$ values (0.1, 0.3, and 0.5) and various Mach

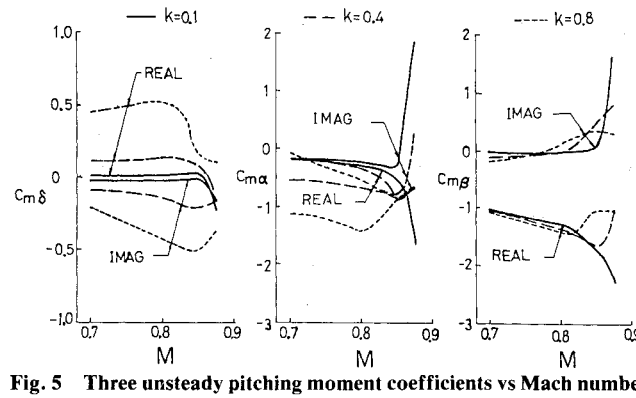


**Fig. 5 Three unsteady pitching moment coefficients vs Mach number for NACA 64A006 airfoil at three reduced frequencies.**

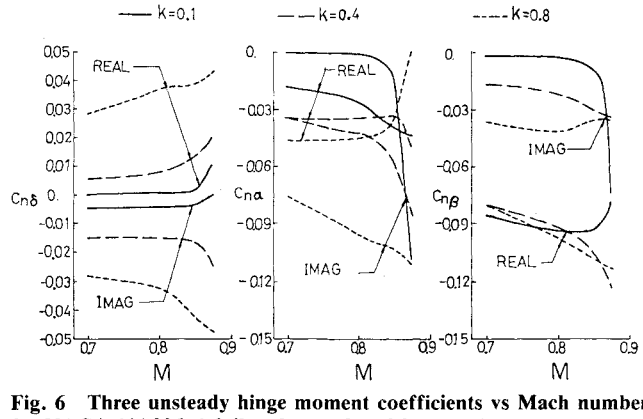


**Fig. 6 Three unsteady hinge moment coefficients vs Mach number for NACA 64A006 airfoil at three reduced frequencies.**

numbers were obtained for both airfoils and plotted in Ref. 30. Only the results for the NACA 64A006 airfoil at $M = 0.85$ are given here (Fig. 7). The flutter boundaries for the three branches: bending-torsion, bending-aileron, and torsion-aileron can be correlated to those for the corresponding binary cases except in the transition zones. Such correlation was made in the study of subsonic cases.[31]

For $\omega_h/\omega_\alpha = 0.1$ in Fig. 7, the flutter speed for the bending-torsion branch increases very slightly with $\omega_\beta/\omega_\alpha$ and the curve approaches asymptote for $\omega_\beta/\omega_\alpha \to \infty$, which corresponds to the bending-torsion binary flutter value. The flutter boundaries for the torsion-aileron and bending-aileron branches appear in the regions of $\omega_\beta/\omega_\alpha < 0.92$ and 0.18, respectively.

For $\omega_h/\omega_\alpha = 0.3$ and 0.5, the flutter boundaries for the torsion-aileron branches are not too much different from those for $\omega_h/\omega_\alpha = 0.1$. However, the two boundaries for bending-torsion and bending-aileron branches become continuous curves, each with a transition portion.

The resulting curves obtained for all other Mach numbers for both airfoils[30] show the trends similar to those found in Fig. 7.

A common means to eliminate the flutter boundaries for the bending-aileron and the torsion-aileron branches is to use aileron mass balance or high aileron pitch stiffness. For a modern aircraft with power-operated irreversible controls, the value of $\omega_\beta/\omega_\alpha$ is much higher than, say, 1.0 and thus the flutter boundaries for the two aileron associated branches do not exist. In the following analyses, $\omega_\beta/\omega_\alpha$ values considered were 0.8 and 1.5, respectively, such that the flutter boundaries for the bending-aileron branch is totally avoided but those for the torsion-aileron branch still exist at $\omega_\beta/\omega_\alpha = 0.8$.

It is noted that the flutter speed for the bending-aileron branch on Fig. 7 would be too low to match the selected Mach number unless the torsional stiffness or $\omega_\alpha$ is very high. It is also noted that $\omega_\beta/\omega_\alpha$ for a business jet could be below 1 and it is usually equal to or greater than 1 for fighters.

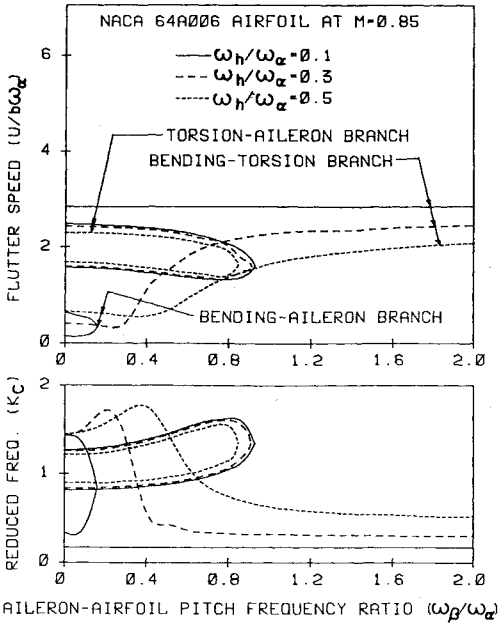


**Fig. 7 Effect of aileron-airfoil pitch frequency ratio on flutter speed for three different airfoil plunge-pitch frequency ratios; $x_\alpha = 0.2$, $r_\alpha = 0.5$, $a_h = -0.2$, $x_\beta = 0.008$, $r_\beta = 0.06$, and $\mu = 50$.**

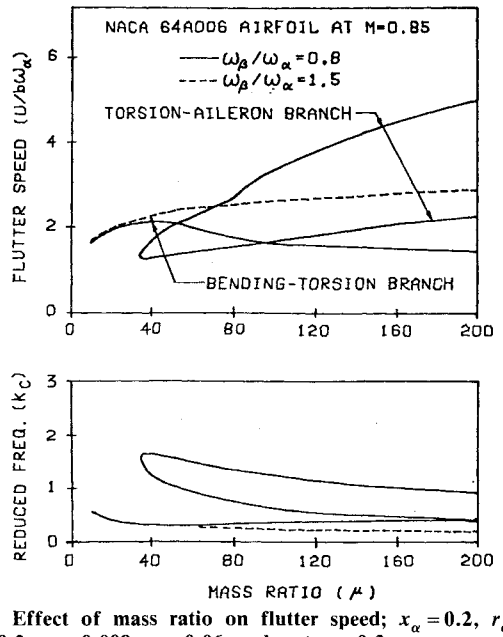


**Fig. 8 Effect of mass ratio on flutter speed; $x_\alpha = 0.2$, $r_\alpha = 0.5$, $a_h = -0.2$, $x_\beta = 0.008$, $r_\beta = 0.06$, and $\omega_h/\omega_\alpha = 0.3$.**

### Effect of Mass Ratio $\mu$

The curves for the flutter speed vs mass ratio $\mu$ for two $\omega_\beta/\omega_\alpha$ values, 0.8 and 1.5, and various Mach numbers were obtained for both airfoils.[30] Only the results for the NACA 64A006 airfoil at $M = 0.85$ are shown here (Fig. 8).

For $\omega_\beta/\omega_\alpha = 1.5$, the flutter speed for the bending-torsion branch increases with $\mu$ in a fashion similar to that for bending-torsion binary flutter. The flutter boundaries for the two aileron associated branches are absent.

For $\omega_\beta/\omega_\alpha = 0.8$, the flutter speed for the bending-torsion branch first increases and then decreases gradually as $\mu$ increases, due to the effect of the aileron motion. Two flutter boundaries for the torsion-aileron branch appear at $\mu > 35$ and both increase as $\mu$ increases.

### Effect of the Position of Airfoil Mass Center $x_\alpha$

The curves for the flutter speed vs $x_\alpha$ ranging from $-0.2$ to 0.4 for two $\omega_\beta/\omega_\alpha$ values, 0.8 and 1.5, were obtained for the

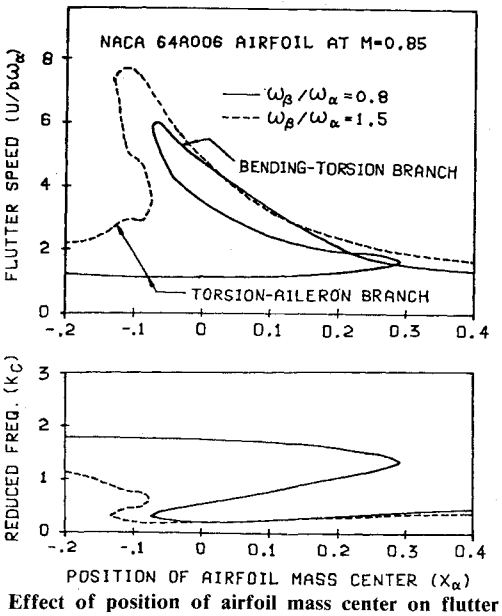


**Fig. 9 Effect of position of airfoil mass center on flutter speed; $r_\alpha = 0.5$, $a_h = -0.2$, $x_\beta = 0.008$, $r_\beta = 0.06$, $\mu = 50$, and $\omega_h/\omega_\alpha = 0.3$.**

MBB A-3 and the NACA 64A006 airfoils at $M = 0.765$ and 0.85, respectively.[30] Only the results for the NACA 64A006 at $M = 0.85$ are shown here (Fig. 9).

For $\omega_\beta/\omega_\alpha = 1.5$, the flutter speed for the bending-torsion branch increases as the mass center moves forward. The flutter boundary for the torsion-aileron branch only appears when $x_\alpha < -0.08$. The sharp turn at the top of the curve marks the transition between the two branches. The flutter boundary for the bending-aileron branch is absent.

For $\omega_\beta/\omega_\alpha = 0.8$, the flutter boundaries take similar trends as those for $\omega_\beta/\omega_\alpha = 1.5$. The transition between the bending-torsion and torsion-aileron branches occur near the top of the curve. The tip on the right of the flutter boundary for the torsion-aileron branch extends to $x_\alpha = 0.29$.

It is physically clear that when an airfoil oscillates with only a single pitching DOF (first natural mode), the forward movement of the mass center stabilizes the airfoil. Such stabilizing effect is also evident in the present flutter speed curves for the bending-torsion branch of a 3DOF system.

### Effect of the Position of Elastic Axis $a_h$

The curves for the flutter speed vs $a_h$ ranging from $-0.5$ to 0 for two $\omega_\beta/\omega_\alpha$ values, 0.8 and 1.5, were obtained for the NACA 64A006 and the MBB A-3 airfoils at $M = 0.85$ and 0.765, respectively.[30] Only the results for the NACA 64A006 airfoil are shown here (Fig. 10).

For $\omega_\beta/\omega_\alpha = 1.5$, the flutter speed for the bending-torsion branch increases as the elastic axis moves forward. The flutter boundary for the torsion-aileron branch appears in the form of a loop in the region of $a_h < -0.47$.

For $\omega_\beta/\omega_\alpha = 0.8$, the flutter boundary for the bending-torsion branch assumes a similar trend as that of the former case. The loop-shaped boundary for the torsion-aileron branch extends to $a_h = -0.14$. The boundaries for the bending-aileron branch disappear in both cases.

The forward movement of the elastic axis has the same stabilizing effect as that of the mass center. Thus, the trend of the flutter boundaries of the bending-torsion branch observed in Fig. 10 is quite similar to that in Fig. 9.

### Effect of the Position of Aileron Mass Center $x_\beta$

The curves for the flutter speed vs $x_\beta$ ranging from 0 to 0.02 for two $\omega_\beta/\omega_\alpha$ values, 0.8 and 1.5, were obtained for the NACA 64A006 and the MBB A-3 airfoils at $M = 0.85$ and 0.765, respectively.[30] Only the results for the NACA 64A006 airfoil are shown here (Fig. 11).

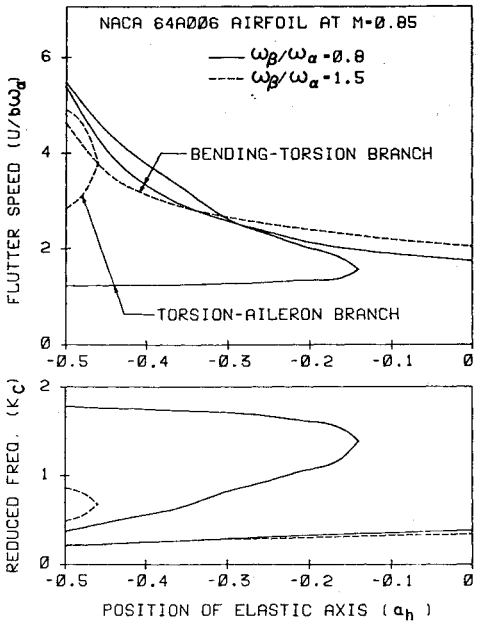


**Fig. 10 Effect of position of elastic axis on flutter speed; $x_\alpha = 0.2$, $r_\alpha = 0.5$, $x_\beta = 0.008$, $r_\beta = 0.06$, $\mu = 50$, and $\omega_h/\omega_\alpha = 0.3$.**

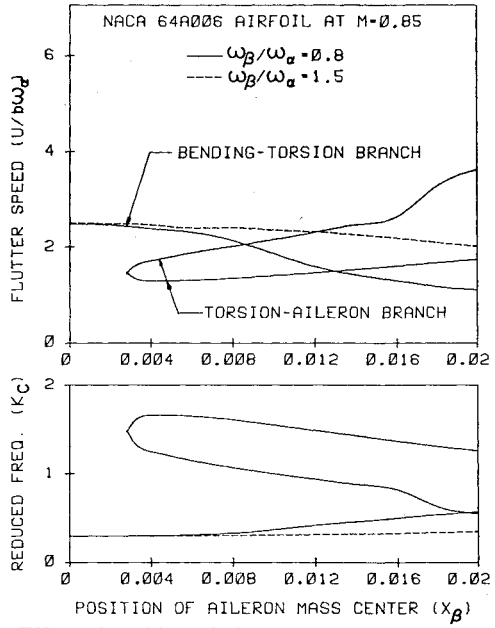


**Fig. 11 Effect of position of aileron mass center on flutter speed; $x_\alpha = 0.2$, $r_\alpha = 0.5$, $a_h = -0.2$, $r_\beta = 0.06$, $\mu = 50$, and $\omega_h/\omega_\alpha = 0.3$.**

For $\omega_\beta/\omega_\alpha = 1.5$, only the flutter boundaries for the bending-torsion branch appear. The flutter speed decreases slightly as $x_\beta$ increases. For $\omega_\beta/\omega_\alpha = 0.8$, the flutter speed for the bending-torsion branch decreases with $x_\beta$ more pronouncedly than that for $\omega_\beta/\omega_\alpha = 1.5$. The drop in flutter speed at $x_\beta = 0.02$ is obviously due to increased aileron response. For $\omega_\beta/\omega_\alpha = 0.8$, the plunge-pitch-aileron amplitude ratios are 1:0.18:0.10, 1:0.10:0.17, 1:0.065:0.62, for $x_\beta = 0$, 0.008, and 0.02, respectively. For $\omega_\beta/\omega_\alpha = 1.5$, such ratios are 1:0.08:0.061,1:0.13:0.092, and 1:0.076:0.21 for $x_\beta = 0$, 0.008, and 0.02, respectively. For $\omega_\beta/\omega_\alpha = 0.8$, the phase lags for plunge-pitch and plunge-aileron are 0.10 and 1.96, −0.10 and 0.70, and −0.30 and 0.25 for $x_\beta = 0$, 0.008, and 0.02, respectively. For $\omega_\beta/\omega_\alpha = 1.5$, such two phase lags are 0.20 and 1.93, 0.14 and 0.74, and −0.003 and 0.31 for $x_\beta = 0$, 0.008, and 0.02, respectively. Although both curves are originally labeled as bending-torsion branch at low $x_\beta$ values, they gradually transform into bending-aileron branch as $x_\beta$ increases.

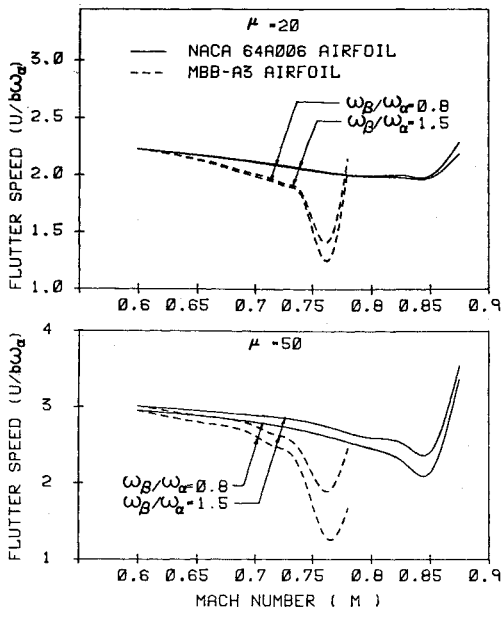


**Fig. 12 Effect of Mach number on flutter speed for both airfoils for two mass ratios: a) $\mu = 20$ and b) $\mu = 50$; $x_\alpha = 0.2$, $r_\alpha = 0.5$, $a_h = -0.2$, $x_\beta = 0.008$, $r_\beta = 0.06$, and $\omega_h/\omega_\alpha = 0.3$.**

For $\omega_\beta/\omega_\alpha = 0.8$, the flutter boundary for the torsion-aileron branch appears only at $x_\beta > 0.003$. The flutter boundary for the bending-aileron branch is absent.

It may be seen that the forward movement of the aileron mass center can not only eliminate the flutter boundary for the torsion-aileron branch (at $x_\beta > 0.003$ in this case), but also can increase the flutter speed of the bending-torsion branch. The advantage of using aileron mass balance is seen in this case.

### Effect of Mach Number ($M$)

Results for the flutter speed vs Mach number were plotted for both airfoils for $\mu = 20$ and 50 in Fig. 12. The curves were plotted for two values of $\omega_\beta/\omega_\alpha$, 0.8 and 1.5. All these curves are for the bending-torsion branch only.

For $\omega_\beta/\omega_\alpha = 1.5$ and for the present values assumed for the other aeroelastic parameters, only the flutter boundaries for the bending-torsion branch are present. Those for the other two aileron related branches are absent. For $\omega_\beta/\omega_\alpha = 0.8$, the flutter boundaries for the bending-aileron branch are absent and those for the torsion-aileron branch are lower than those for the bending-torsion branch. However, the flutter speed curves for the bending-torsion branch at $\omega_\beta/\omega_\alpha = 0.8$ were still plotted in Fig. 12 for the purpose of comparison with those at $\omega_\beta/\omega_\alpha = 1.5$. As noted earlier, for a modern aircraft with power-operated irreversible controls the value of $\omega_\beta/\omega_\alpha$ may be much higher than, say, 1.0.

The figure shows that the bottoms of the transonic dips occur in the neighborhood of the design Mach number of 0.765 for the MBB A-3 airfoil and in the neighborhood of $M = 0.85$ for the NACA 64A006 airfoil. In a flutter analysis of the NACA 64A006 airfoil with only plunge and pitch DOF's[10] the transonic dip for the parameter values considered was also found to be near $M = 0.85$.

The figure shows that the mass ratio has a detrimental effect in deepening the transonic dip. This effect was pointed out in Ref. 4.

The transonic dip phenomenon may be explained as a result of the compensating effects of the lift coefficient and the position of the center of pressure.[32] Description of the mechanism of the transonic dip is attempted in the next section. It may also be of interest to point out that each transonic dip in Fig. 12 occurs in the range of Mach numbers where the phase lag of the lift coefficient $c_{l_\alpha}$ becomes

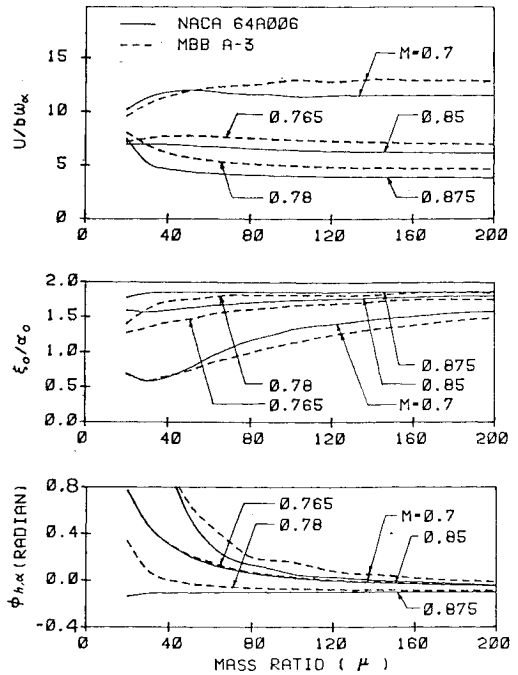


**Fig. 13 Flutter speed and flutter mode (amplitude ratio and phase angle) vs mass ratio for both airfoils for a 2DOF swept wing simulation; $x_\alpha = 1.8$, $r_\alpha = 1.867$, $a_h = -2$, and $\omega_h/\omega_\alpha = 1$.**

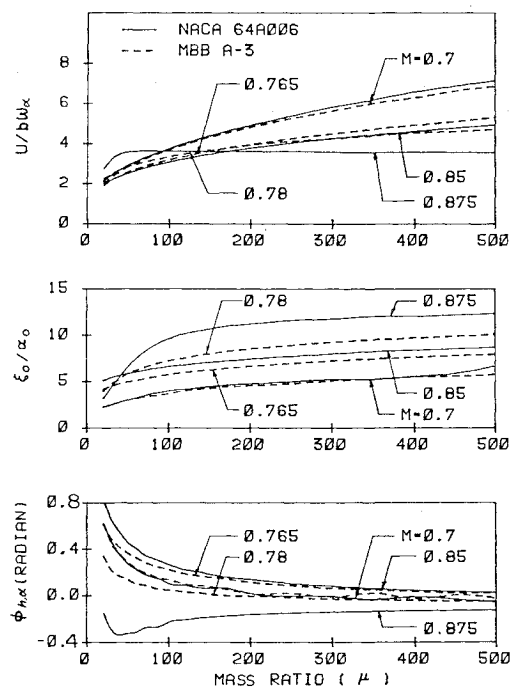


**Fig. 14 Flutter speed and flutter mode (amplitude ratio and phase angle) vs mass ratio for both airfoils for a 2DOF straight wing simulation; $x_\alpha = 0.2$, $r_\alpha = 0.5$, $a_h = -0.2$, and $\omega_h/\omega_\alpha = 0.3$.**

relatively the largest. Similar observation was reported in Refs. 5 and 13.

Results for the flutter speed vs Mach number for other values of the parameters $\omega_h/\omega_\alpha$, $x_\alpha$, $a_h$ are available in Ref. 30.

### Discussion of the Flutter Modes

To study the flutter mode, the case of two DOF's (plunge and pitch) was first considered. The flutter speed, plunge-pitch amplitude ratio, and plunge-pitch phase difference were plotted against the mass ratio in Fig. 13 for both airfoils and

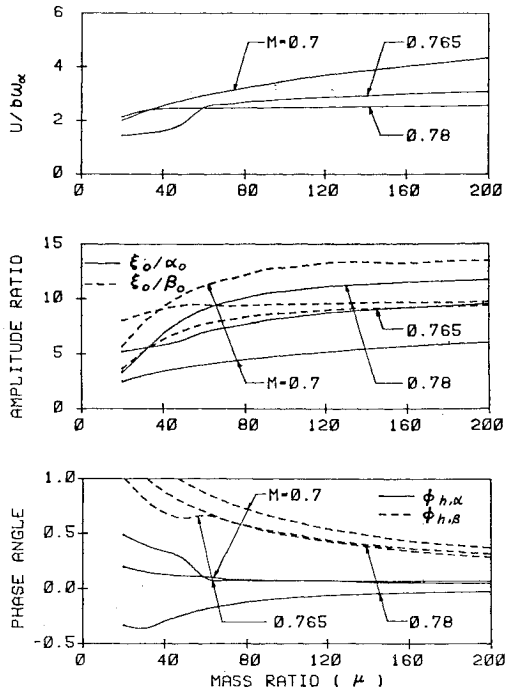


**Fig. 15 Flutter speed and flutter mode (amplitude ratios and phase angles) vs mass ratio for the MBB A-3 airfoil for a 3DOF straight wing simulation; $x_\alpha = 0.2$, $r_\alpha = 0.5$, $a_h = -0.2$, $x_\beta = 0.008$, $r_\beta = 0.06$, $\omega_h/\omega_\alpha = 0.3$, and $\omega_\beta/\omega_\alpha = 1.5$.**

various Mach numbers. The values of the parameters used are the same as those assumed for a NACA 64A010 airfoil in the case of a swept wing simulation in Ref. 13: $x_\alpha = 1.8$; $r_\alpha = 1.867$; $a_h = -2.0$, and $\omega_h/\omega_\alpha = 1.0$.

It is seen that, at the bottoms of the transonic dips ($M = 0.78$ and 0.875 for MBB A-3 and NACA 64A006 airfoils, respectively), the amplitude ratios gradually converge to a constant value of 1.868 (first natural mode) and the phase differences gradually approach zero as the mass ratio becomes larger. There is more bending (change in flutter mode) at higher mass ratios or higher Mach numbers than for lower mass ratios and lower Mach numbers. The phenomenon observed here agrees with that pointed out in Ref. 13.

The parameter values were then changed to $x_\alpha = 0.2$; $r_\alpha = 0.5$; $a_h = -0.2$, and $\omega_h/\omega_\alpha = 0.3$ for the case of a straight wing simulation. The results were plotted in Fig. 14 in the fashion similar to that of Fig. 13.

As shown in Fig. 14, for the NACA 64A006 airfoil, the two flutter speed curves for $M = 0.85$ and 0.875 cross each other at $\mu = 185$. For higher $\mu$ values, the flutter speed for $M = 0.875$ becomes increasingly lower than that for $M = 0.85$ and the bottom of the transonic dip definitely shifts to a Mach number higher than 0.85.

It is seen that for $M = 0.875$ and $\mu > 185$, the amplitude ratio approaches a constant value of 12.86 (first natural mode) and the phase difference decreases to zero as $\mu$ becomes larger.

For the MBB A-3 airfoil the two flutter curves for $M = 0.765$ and 0.78 cross each other at $\mu = 195$. For $M = 0.78$ and $\mu > 195$, the amplitude ratio approaches rather slowly the constant value of 12.86 (first natural mode) and the phase difference decreases to zero as $\mu$ becomes larger.

The MBB A-3 airfoil with three DOF's is then considered. The parameter values are $a_h = -0.2$; $x_\alpha = 0.2$; $r_\alpha = 0.5$; $x_\beta = 0.008$; $r_\beta = 0.06$; $\omega_h/\omega_\alpha = 0.3$; and $\omega_\beta/\omega_\alpha = 1.5$. The results are given in Fig. 15.

At $M = 0.78$, the plunge-pitch and the plunge-aileron pitch amplitude ratios approach two constant values of 12.81 and 10.1, respectively (first natural modes). There is more aileron motion at low mass ratio. The two phase differences approach zero as the mass ratio becomes larger.

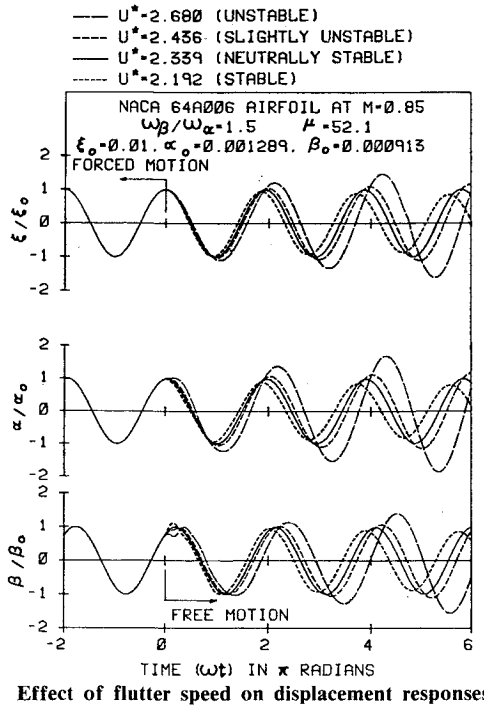


Fig. 16 Effect of flutter speed on displacement responses for the NACA 64A006 airfoil at $M = 0.85$.

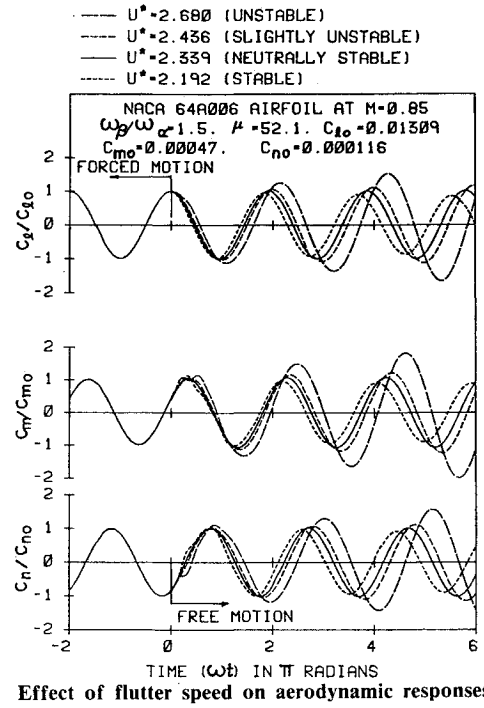


Fig. 17 Effect of flutter speed on aerodynamic responses for the NACA 64A006 airfoil at $M = 0.85$.

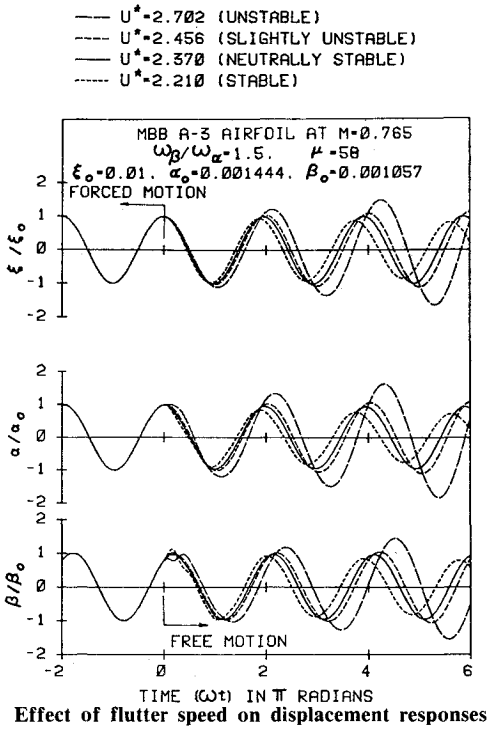


Fig. 18 Effect of flutter speed on displacement responses for the MBB A-3 airfoil at $M = 0.765$.

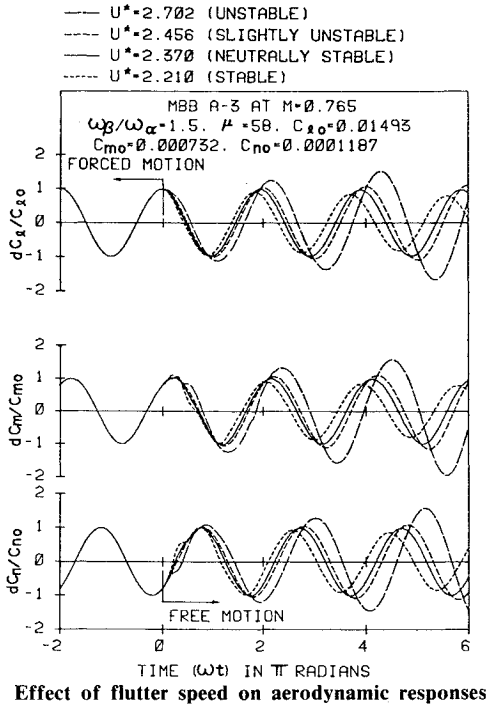


Fig. 19 Effect of flutter speed on aerodynamic responses for the MBB A-3 airfoil at $M = 0.765$.

## Results of Time-Response Analysis

Time-response results were obtained for the NACA 64A006 airfoil at $M = 0.7$ and 0.85 and for the MBB A-3 airfoil at $M = 0.765$, respectively. The parameters are defined as $a_h = -0.2$; $x_\alpha = 0.2$; $r_\alpha = 0.5$; $x_\beta = 0.008$; $r_\beta = 0.06$; $\omega_h/\omega_\alpha = 0.3$; $\omega_\beta/\omega_\alpha = 1.5$; and $k_c = 0.3$.

A time-response analysis was first performed for the NACA 64A006 airfoil at $M = 0.7$. Based on the flutter speed found in a flutter analysis, $U^* = 2.816$ at $\mu = 48$, the neutrally stable responses were indeed obtained.[30]

A time-response analysis was then performed for the NACA 64A006 airfoil at $M = 0.85$. The results for the three displacements and the three aerodynamic forces were plotted in Figs. 16 and 17, respectively. In Fig. 17, $c_{l0}$, $c_{m0}$, and $c_{n0}$ are the amplitudes of $c_l$, $c_m$, and $c_n$, respectively, obtained in the forced harmonic motion.

The airfoil was first forced to oscillate for 5½ cycles in order for the response of the three aerodynamic coefficients to become periodic. The airfoil was then set free and the aeroelastic time-responses were calculated. Based on a flutter solution, $U^* = 2.436$ at $\mu = 52.1$, the time responses were found to be slightly diverging (unstable). The flight speed was then reduced by 10% and the time responses were found to be converging (stable). When the flight speed was reduced by only 4%, the neutrally stable responses were eventually obtained. In the neutrally stable free motion, the frequency was found to be 1% higher than that of the original forcing function.

For the MBB A-3 airfoil at $M=0.765$, the response results for the three displacements and the three aerodynamic forces were plotted in Figs. 18 and 19, respectively. In Fig. 19, $dc_l$ is the differential $c_l$ relative to the mean value of $c_l$ in forced motion; $dc_m$ and $dc_n$ are defined in the same way.

Again, the airfoil was first forced to oscillate for 5½ cycles to obtain the periodic aerodynamic responses. Based on a flutter solution, $U^*=2.456$ at $\mu=58$, the time responses were found to be slightly diverging. The neutrally stable responses were obtained when the flight speed was reduced by 3.5%.

## Concluding Remarks

Based on the present flutter and time-response analyses, the following concluding remarks can be made.

1) As can be seen in Figs. 2 and 3, strong shocks are present at $M=0.875$ and 0.78 for the NACA 64A006 and MBB A-3 airfoils, respectively. Both the steady and unsteady aerodynamic results were obtained by using the LTRAN2-NLR code. Difficulty was, however, encountered when attempting to obtain unsteady results for the NACA 64A006 airfoil at $M=0.9$.

2) In computing the aerodynamic coefficients for all cases, $k_c$ values of up to 1.6 were considered. For a flat plate at $M=0.7$, all nine unsteady aerodynamic coefficients were obtained which agreed reasonably well with the kernel function method results.[30]

3) For the parameter values considered, the results show that the flutter boundaries for the bending-aileron and the torsion-aileron branches disappear when $\omega_\beta/\omega_\alpha$ is approximately greater than 1. The aileron effect on the flutter speed of the bending-torsion branch diminishes gradually as $\omega_\beta/\omega_\alpha$ increases.

4) As seen in Figs. 8-10, the flutter speed for $\omega_\beta/\omega_\alpha=1.5$ increases as the mass ratio becomes larger, as the mass center moves forward, and as the elastic axis moves forward, respectively. It also increases as the radius of gyration of the airfoil becomes larger.[30]

5) As seen in Fig. 11, forward movement of the aileron mass center can not only eliminate the flutter boundaries of aileron associated branches but also increase the flutter speed of the bending-torsion branch.

6) For the sets of parameter values considered and for the NACA 64A006 and MBB A-3 airfoils at $M=0.875$ and 0.78, respectively, each flutter mode converges to its corresponding first natural mode as the mass ratio becomes larger, at a rate faster than those at other Mach numbers considered.

7) For the NACA 64A006 airfoil at $M=0.7$, neutrally stable responses were obtained based on a set of parameter values corresponding to a flutter condition in a separate flutter analysis.[30] For the NACA 64A006 airfoil at $M=0.85$ and the MBB A-3 airfoil at $M=0.765$, neutrally stable responses were obtained based on the flight speed 4% and 3.5% lower than the respective flutter speeds found in the separate flutter analyses. Such small differences have recently been removed by increasing the number of time-steps per cycle of response motion.[33]

8) Including viscous effects in transonic flow calculations would result in a less strong shock wave located further upstream than inviscid methods indicate. A study is currently being conducted that includes viscous effects such as shock-boundary layer interaction and aft-decambering for the prediction of flutter condition.

9) Recently, two-dimensional codes were developed without the restrictions of low frequency[13,20,21] and small disturbance.[22] The viscous effect was accounted for by using a viscous ramp method.[21] A three-dimensional unsteady transonic code has also been developed.[23] These new developments will be very valuable tools for exploring the field of transonic aeroelasticity.

10) A logical extension of the present development is to include terms in the response equations of motion to simulate the active control forces for the application of flutter suppression.

## Acknowledgments

This research is partially sponsored under AFOSR Grant 78-3523. Many original ideas and valuable suggestions from J.J. Olsen and technical assistance from L.J. Huttsell, both of Air Force Wright Aeronautical Laboratories, are gratefully acknowledged. The authors also acknowledge NLR, W.F. Ballhaus, and P.M. Goorjian for making LTRAN2-NLR available. Help from J.T. Batina is also acknowledged.

## References

[1] Ballhaus, W.F. and Bridgeman, J.O., "Numerical Solution Techniques for Unsteady Transonic Problems," AGARD Rept. 679, June 1980, pp. 16-1-16-24.

[2] Ashley, H., "Role of Shocks in the 'Sub-Transonic' Flutter Phenomenon," *Journal of Aircraft*, Vol. 17, March 1980, pp. 187-197.

[3] Yang, T.Y., Guruswamy, P., and Striz, A.G., "Application of Transonic Codes to Flutter Analysis of Conventional and Supercritical Airfoils," *Proceedings of AIAA Dynamics Specialists Conference*, Atlanta, Ga., April 1981, pp. 332-342; see also *Journal of Aircraft*, Vol. 19, March 1982, pp. 211-220.

[4] Mykytow, W.J., "A Brief Overview of Transonic Flutter Problems," *Unsteady Airloads in Separated and Transonic Flow*, AGARD-CP-226, April 1977, pp. 11-1-11-11.

[5] Zwaan, R.J., "Aeroelastic Problems of Wings in Transonic Flow," NLR-MP-81005U, National Aerospace Laboratory, the Netherlands, 1981.

[6] Farmer, M.G. and Hanson, P.W., "Comparison of Supercritical and Conventional Wing Flutter Characteristics," *Proceedings of AIAA/ASME/SAE 17th Structures, Structural Dynamics, and Materials Conference*, King of Prussia, Pa., April 1976, pp. 608-614; see also NASA TM X-72837, May 1976.

[7] Rizzetta, D.P., "Transonic Flutter Analysis of a Two-Dimensional Airfoil," AFFDL-TM-77-64-FBR, July 1977.

[8] Traci, R.M., Albano, E.D., and Farr, J.L., "Small Disturbance Transonic Flows About Oscillating Airfoils and Planar Wings," AFFDL-TR-75-100, June 1975.

[9] Ballhaus, W.F. and Goorjian, P.M., "Implicit Finite-Difference Computations of Unsteady Transonic Flows About Airfoils," *AIAA Journal*, Vol. 15, Dec. 1977, pp. 1728-1735.

[10] Yang, T.Y., Guruswamy, P., Striz, A.G., and Olsen, J.J., "Flutter Analysis of a NACA 64A006 Airfoil in Small Disturbance Transonic Flow," *Journal of Aircraft*, Vol. 17, April 1980, pp. 225-232.

[11] Yang, T.Y., Striz, A.G., and Guruswamy, P., "Flutter Analysis of a Two-Degree-of-Freedom MBB A-3 Supercritical Airfoil in Two-Dimensional Transonic Flow," *Proceedings of AIAA/ASME/ASCE/AHS 21st Structures, Structural Dynamics, and Materials Conference*, Seattle, Wash., May 1980, pp. 434-443; see also *Journal of Aircraft*, Vol. 18, Oct. 1981, pp. 887-890.

[12] Isogai, K., "On the Transonic-Dip Mechanism of Flutter of a Sweptback Wing," *AIAA Journal*, Vol. 17, July 1979, pp. 793-795.

[13] Isogai, K., "Numerical Study of Transonic Flutter of a Two-Dimensional Airfoil," NAL TR-617T, National Aerospace Laboratory, Tokyo, Japan, July 1980.

[14] McGrew, J.A., Giesing, J.P., Pearson, R.M., Zuruddin, K., Schmidt, M.E., and Kalman, T.P., "Supercritical Wing Flutter," AFFDL-TR-78-37, March 1978.

[15] Eastep, F.E. and Olsen, J.J., "Transonic Flutter Analysis of a Rectangular Wing with Conventional Airfoil Sections," *AIAA Journal*, Vol. 18, Oct. 1980, pp. 1159-1164.

[16] Ballhaus, W.F. and Goorjian, P.M., "Computation of Unsteady Transonic Flows by the Indicial Method," *AIAA Journal*, Vol. 16, Feb. 1978, pp. 117-124.

[17] Rizzetta, D.P., "Time-Dependent Responses of a Two-Dimensional Airfoil in Transonic Flow," *AIAA Journal*, Vol. 17, Jan. 1979, pp. 26-32.

[18] Guruswamy, P. and Yang, T.Y., "Aeroelastic Time Response Analysis of Thin Airfoils by Transonic Code LTRAN2," *Journal of Computers and Fluids*, Vol. 9, Dec. 1981, pp. 409-425; see also AFFDL-TR-79-3077, June 1979.

[19] Houwink, R. and van der Vooren, J., "Results of an Improved Version of LTRAN2 for Computing Unsteady Airloads on Airfoils Oscillating in Transonic Flow," AIAA Paper 79-1553, July 1979.

[20] Rizzetta, D.P. and Chin, W.C., "Effect of Frequency in Unsteady Transonic Flow," *AIAA Journal,* Vol. 17, July 1979, pp. 779-781.

[21] Rizzetta, D.P. and Yoshihara, H., "Computations of the Pitching Oscillation of a NACA 64A010 Airfoil in the Small Disturbance Limit," AIAA Paper 80-0128, Jan. 1980.

[22] Goorjian, P.M., "Implicit Computations of Unsteady Transonic Flow Governed by the Full Potential Equation in Conservation Form," AIAA Paper 80-0150, Jan. 1980.

[23] Borland, C., Rizzetta, D., and Yoshihara, H., "Numerical Solution of Three-Dimensional Unsteady Transonic Flow Over Swept Wings," AIAA Paper 80-1369, July 1980.

[24] Fung, Y.C., *Theory of Aeroelasticity,* Dover Publications, Inc., New York, 1969, Secs. 6.10 and 6.11.

[25] Davis, S.S. and Malcolm, G.N., "Experiments in Unsteady Transonic Flow," *Proceedings of AIAA/ASME/ASCE/AHS 20th Structures, Structural Dynamics, and Materials Conference,* St. Louis, Mo., April 1979.

[26] Bathe, K.J. and Wilson, E.L., *Numerical Methods in Finite Element Analysis,* Prentice-Hall, Inc., Englewood Cliffs, New Jersey, 1976, Chaps. 8 and 9.

[27] Bland, S.R., "AGARD Two-Dimensional Aeroelastic Configurations," AGARD-AR-156, Aug. 1979.

[28] Tijdeman, H., "Investigation of the Transonic Flow Around Oscillating Airfoils," NLR-TR-77090U, National Aerospace Laboratory, the Netherlands, Dec. 1977.

[29] Bucciantini, G., Oggiano, M.S., and Onorato, M., "Supercritical Airfoil MBB A-3, Surface Pressure Distributions, Wake and Boundary Condition Measurements," AGARD Advisory Rept. 138, May 1979, pp. A8-1-A8-25.

[30] Chen, C.H., "Flutter and Time Response Analyses of Three Degree of Freedom Airfoils in Transonic Flow," Ph.D. Thesis, Purdue University, West Lafayette, Ind., July 1981.

[31] Theodorsen, T. and Garrick, I.E., "Flutter Calculations in Three Degrees of Freedom," NACA Rept. 741, 1942.

[32] Hitch, H.P.Y., "Comment on 'Flutter Analysis of NACA 64A006 Airfoil in Small Disturbance Transonic Flow,'" Yang, T.Y., Guruswamy, P., Striz, A.G., and Olsen, J.J., "Reply by Authors to H.P.Y. Hitch," *Journal of Aircraft,* Vol. 18, Feb. 1981, pp. 158-160.

[33] Yang, T.Y. and Batina, J.T., "Transonic Time-Response Analysis of Three DOF Conventional and Supercritical Airfoils," *Proceedings of AIAA/ASME/ASCE/AHS 23rd Structures, Structural Dynamics, and Materials Conference,* New Orleans, La., May 1982, pp. 250-266.

*From the AIAA Progress in Astronautics and Aeronautics Series..*

**AEROACOUSTICS:**

**JET NOISE; COMBUSTION ANDCORE ENGINE NOISE**—v. 43
**FAN NOISE AND CONTROL; DUCT ACOUSTICS; ROTOR NOISE**—v. 44
**STOL NOISE;AIRFRAME AND AIRFOIL NOISE**—v. 45
**ACOUSTIC WAVE PROPAGATION;**
**AIRCRAFT NOISE PREDICTION;**
**AEROACOUSTIC INSTRUMENTATION**—v. 46

*Edited by Ira R. Schwartz, NASA Ames Research Center, Henry T. Nagamatsu, General Electric Research and Development Center, and Warren C. Strahle, Georgia Institute of Technology*

The demands placed upon today's air transportation systems, in the United States and around the world, have dictated the construction and use of larger and faster aircraft. At the same time, the population density around airports has been steadily increasing, causing a rising protest against the noise levels generated by the high-frequency traffic at the major centers. The modern field of aeroacoustics research is the direct result of public concern about airport noise.

Today there is need for organized information at the research and development level to make it possible for today's scientists and engineers to cope with today's environmental demands. It is to fulfill both these functions that the present set of books on aeroacoustics has been published.

The technical papers in this four-book set are an outgrowth of the Second International Symposium on Aeroacoustics held in 1975 and later updated and revised and organized into the four volumes listed above. Each volume was planned as a unit, so that potential users would be able to find within a single volume the papers pertaining to their special interest.

*v.43—648 pp., 6 x 9, illus.* $19.00 Mem. $40.00 List
*v. 44—670 pp., 6 x 9, illus.* $19.00 Mem. $40.00 List
*v. 45—480 pp., 6 x 9, illus.* $18.00 Mem. $33.00 List
*v. 46—342 pp., 6 x 9, illus.* $16.00 Mem. $28.00 List

*For Aeroacoustics volumes purchased as a four-volume set:* $65.00 Mem. $125.00 List

TO ORDER WRITE: Publications Dept., AIAA, 1290 Avenue of the Americas, New York, N.Y. 10019